RESEARCH ARTICLE

Narrowband SIW-SSPP Hybrid Bandpass Filter With Compact Profile at Ka-Band

BAOQING ZHANG[1], ZHAOLIN LI[1], MENGFA WANG[1], HAOTIAN LING[2], YIMING WANG[1], XIJIAN ZHANG[1], WEIHONG LIU[3], VICTOR QI[4], KUNFENG CHEN[5], GONGBIN TANG[5], AIMIN SONG[1,6], (Senior Member, IEEE), AND YIFEI ZHANG[1], (Member, IEEE)

[1]Shandong Technology Center of Nanodevices and Integration, School of Microelectronics, Shandong University, Jinan 250100, China
[2]QiLu Aerospace Information Research Institute, Jinan 250101, China
[3]Department of Electronic Engineering, Xi'an University of Posts and Telecommunications, Xi'an, Shaanxi 710121, China
[4]Design Center of AKMMV, Nansha, Guangzhou 511400, China
[5]State Key Laboratory of Crystal Materials, Institute of Novel Semiconductors, Shandong University, Jinan 250100, China
[6]Department of Electrical and Electronic Engineering, The University of Manchester, M13 9PL Manchester, U.K.

Corresponding author: Yifei Zhang (yifeizhang@sdu.edu.cn)

ABSTRACT In this paper, a narrowband bandpass filter comprising substrate integrated waveguide (SIW) and spoof surface plasmon polaritons (SSPPs) is proposed, achieving miniaturization and low insertion loss at Ka-band. SIWs and SSPPs exhibit low and high cut-off responses, respectively, which can be combined for filtering functionalities. By designing I-shaped SSPP structures with large effective length, the cut-off frequencies of SIW and SSPPs can be tailed to converge at a certain frequency for the narrowband filter, where the SIW mode functions as a quasi-evanescent mode, and the mode impedance ramps fast. A sharp funnel-shaped transition is designed to connect SIW with a large impedance and 50-Ω microstrip line for low insertion loss and a compact profile. In addition, no transitional SSPP structures are desired in the proposed devices, which further shortens the profile dimension. To verify our design, a hybrid filter at 30 GHz is fabricated and characterized. The measured insertion loss is as low as 1.5 dB, and the 3-dB bandwidth is as narrow as 3%, which shows good consistency with the simulation. The proposed SIW-SSPP device has a low profile of $0.70 \lambda \times 0.38 \lambda$ and may find important applications in frequency division multiplexing.

INDEX TERMS Bandpass filter, miniaturization, narrowband, substrate integrated waveguide (SIW), spoof surface plasmon polariton (SSPP).

I. INTRODUCTION

Substrate integrated waveguide (SIW) is a waveguide-like structure fabricated in a dielectric substrate with two rows of periodic metallic vias connecting the top and bottom metallic conductors [1], [2]. It preserves most of the advantages of air-filled waveguides, such as low loss, high power handling capability, and high electromagnetic compatibility, and achieves low profile, low weight, and simple circuit integration, enabling many important applica-

The associate editor coordinating the review of this manuscript and approving it for publication was Qilian Liang.

tions in microwave circuits [3], filters [4], antennas [5], and front-end modules [6]. Recently, SIW-spoof surface plasmon polariton (SSPP) hybrid devices have gained great interest [7], [8], [9], [10], [11], [12], [13]. Surface plasmon polaritons (SPPs) are surface waves propagating along the interface between a dielectric and a noble metal at optical frequencies, where the metal shows plasmonic properties [14]. However, the noble metals are typically considered as perfect electric conductors (PECs) below infrared frequencies, and thus cannot guide SPPs at terahertz and microwave frequencies [15]. In 2004, Pendry theoretically demonstrated SPP-like surface waves on periodic metal holes [16], which is typically

referred to as SSPPs and shows a high cut-off response at its effective plasmon frequency as its optical counterparts [17]. In 2011, 2-D SSPP structure was demonstrated by Kats et al, which consists of periodic vertical grooves on a metal plate [18]. In 2014, 1-D SSPP structure, i.e., a single metal line with periodic planar corrugations, was proposed by Ma et al. [19], which can be friendly integrated with the conventional transmission lines, such as microstrip lines (MSLs) and co-planar waveguides (CPWs) [20]. In 2015, a broadband bandpass filter with SIW and SSPP cascaded in series was reported, which consists of a high pass filter induced by the TE_{10} mode of SIW and a low pass filter on SSPPs [8]. Since then, several kinds of SIW-SSPP hybrid filters have been investigated based on the cut-off responses of SIWs and SSPPs.

In 2017, 2-D SSPPs with periodic vertical blind vias designed on the bottom electrode of SIW were demonstrated in multilayer circuits, which enables the first SIW-SSPP hybrid filter with a wide passband ranging from 16.1 to 25.4 GHz [7]. Later, 1-D SSPPs were designed in the top electrode of SIWs, and a SIW-SSPP hybrid filter with a 3-dB bandwidth of 44%, i.e., 7.3-11.2 GHz, was reported [9]. To achieve low profiles, this kind of 1-D SSPPs has been investigated in half-mode SIW (HMSIW) and enables broadband hybrid filters with a 3-dB bandwidth of up to 70% [11], [12], [13]. In the last two years, dumbbell SSPP slots were proposed for the hybrid filters with a 3-dB bandwidth of >19.6% [21], [22]. It is interesting to note that these reported SIW-SSPP hybrid filters are wideband devices with TE_{10} mode [7], [8], [9], [10], [11], [12], [13], [21], [22]. To match the mode profiles of transition lines and SIWs, the corresponding transitions are typically composed of long transmission line tapers [7], [8], [9], [10], [11], [12], [13], [21], [22]. These long tapers have been widely used in SIW circuits for decades [5]. In addition, transitional SSPP structures are required to match the momentum of transmission lines and SSPPs gradually for low attenuation [23]. However, the long MSL-to-SIW tapers and transitional SSPP structures significantly enlarge the filter length, which typically makes the electrical length of hybrid filters in several wavelength scales [7], [8], [9], [10], [11], [12], [13], [21], [22].

In this paper, a novel SIW-SSPP hybrid bandpass filter is designed and demonstrated, achieving a 3-dB bandwidth of as narrow as 3%, a low insertion loss of 1.5 dB at 30 GHz, and the lowest profile to the best of the authors' knowledge among the SIW-SSPP filters. To make the cut-off frequencies of SIW and SSPPs approach, I-shaped SSPP slots are designed in the top SIW electrode and thus provide a larger effective length than the typical rectangular slots. Differing from the reported wideband hybrid filter, the proposed filter is based on a quasi-evanescent mode at the SIW cut-off frequencies, whose mode impedance is as large as several hundred ohms. In this case, a sharp funnel-shaped taper is designed to connect MSLs and proposed filter for impedance matching. The beauty of this design is that no transitional SSPP structures

are desired, which significantly reduces the device length down to sub-wavelength scales. The paper is organized as follows. In Section II, the design principle and equivalent circuit model of the hybrid filter are discussed, and the short taper transition is designed and optimized. Then, experiment details will be discussed in Section III. Finally, the conclusion will be given in the last section.

II. DESIGN AND SIMULATION

Similar to the classic rectangular metallic waveguide, the fundamental mode of SIW is TE_{10} mode, the propagation constant of SIW can be expressed as

$$\beta_{SIW} \approx \sqrt{\varepsilon_r \mu_r k_0^2 - \left(\frac{\pi}{W_{siw}}\right)^2}, \qquad (1)$$

where W_{siw} represents the width of SIW, ε_r and μ_r are the relative permittivity and permeability of the substrate, and k_0 is the wave number in free space [24]. In this case, the corresponding cut-off frequency is given by

$$f_{c-siw} \approx \frac{c_0}{2W_{siw}\sqrt{\varepsilon_r}}, \qquad (2)$$

where c_0 represents the free-space light speed [25]. On the other hand, the dispersion properties of SSPPs are typically determined by the dimensions of the periodic grooves as

$$\beta_{SSPP} = k_0 \sqrt{E_{eff} + \frac{W_{spp1}^2}{P_{spp2}} E_{eff} tan^2 \left(k_0 \sqrt{E_{eff}} L_{spp}\right)}, \quad (3)$$

where W_{spp1} is the width of the groove, P_{spp} is the period of the grooves, L_{spp} is the groove length, E_{eff} is the effective permittivity for metal grooves [26]. The cut-off frequency of SSPPs can be obtained by

$$f_{c-spp} = \frac{c_0}{4L_{spp}\sqrt{\varepsilon_{eff}}}. \qquad (4)$$

According to the above equations, it can be found that the SIWs have a low cut-off response, and SSPPs have a high cut-off response. Combining SIWs and SSPPs can obtain bandpass filters, whose bandwidth can be tailed by sweeping the dimensions of SIW and SSPP structures. In this work, the proposed SIW-SSPP hybrid filter is designed on a 10-mil thick Rogers 5880 substrate, which has a relative permittivity of 2.2 and a loss tangent of less than 0.0009. The laminated copper layer has a thickness of 18 μm. The center frequency of the passband is chosen at around 30 GHz, which is of great importance for the fifth generation (5G) communication applications. Ansys High Frequency Structural Simulator (HFSS) is employed for the detailed analysis in the following sections. Unlike the optical SPPs in the optical domain, copper is typically treated as a good conductor with a relative permittivity of 1 and a bulk conductivity of 5.8e7 S/m at microwave frequencies in our simulation.
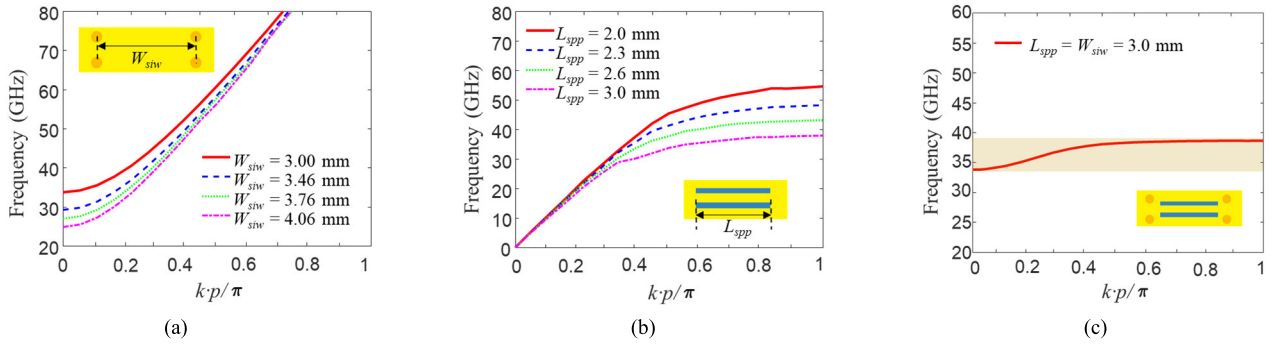
FIGURE 1. Eigen mode simulation and analysis. (a) Dispersion relation of SIWs with low cut-off response, (b) dispersion relation of SSPPs with high cut-off response, and (c) dispersion relation of SIW-SSPP hybrid structure exhibiting both cut-off responses.

TABLE 1. Dimensions of the Proposed Hybrid Filter at 30 GHz.

W_{siw}	T_{copper}	L_{ms}	W_{ms}
3.76 mm	18 μm	3 mm	0.66 mm
L_{spp}	L_{spp1}	P_{spp}	L_{siw}
2.30 mm	0.43 mm	0.70 mm	6.4 mm
W_{spp1}	W_{spp2}	L_t	W_t
0.16 mm	0.10 mm	0.20 mm	0.10 mm
d	P_{siw}	L_{spp2}	
0.4 mm	0.91 mm	0.38 mm	

A. EIGEN MODE SIMULATION

To precisely obtain the cut-off frequencies, eigen mode simulation is performed for SIW, SSPP, and SIW-SSPP hybrid unit cells, which are depicted as the inserts in Fig. 1. The dispersion relation of SIWs is illustrated in Fig. 1(a). It can be seen that the cut-off frequency f_{c-siw} increases as the SIW width W_{siw} decreases, showing good consistency with Equation (2). For instance, the SIW cut-off frequency is 33.6 GHz at $W_{siw} = 3$ mm. Figure 1(b) shows the dispersion relation of the conventional SSPPs with rectangular grooves. As the groove length L_{spp} enlarges, the high cut-off frequency of SSPPs f_{c-spp} decreases. At $L_{spp} = 3$ mm, the corresponding cut-off frequency is 38 GHz for the SSPPs with a period $p = 0.7$ mm. In this case, it is easy to get a bandpass filter by combining SIWs and SSPPs, whose bandwidth narrows as the cut-off frequencies of SIW and SSPP structures approach. Ideally, at $W_{siw} = L_{spp} = 3.0$ mm and $P_{spp} = 0.7$ mm, the passband of a SIW-SSPP filter should be from 33.6 to 38 GHz approximately, i.e., as broad as 12%.

In the practical SIW fabrication, L_{spp} should be much smaller than W_{siw}. Firstly, the metallic vias for SIW sidewalls typically have annual rings of 0.1-0.2 mm for surface finish [27], which significantly limits L_{spp} at high frequencies as the device size gets smaller. Secondly, the long SSPP slots near the SIW sidewall will introduce additional leakage loss for SIWs, which is not preferred for filter design. In this case, narrowband SIW-SSPP hybrid filter cannot be obtained with simple rectangular slots for SSPPs. To overcome this limit, I-shaped slots are designed to lower the SSPP cut-off frequency f_{c-spp} in this work, as illustrated in Fig. 2(a). L_{spp1} and
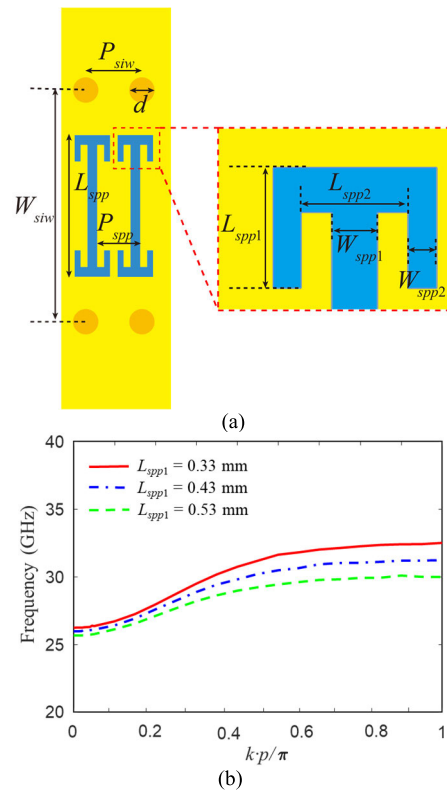
FIGURE 2. SIW-SSPP unit cell for simulation. (a) Top view of hybrid structure and its zoom-in picture for I-shaped slot, (b) Dispersion curves with L_{spp1} variation.

L_{spp2} are induced to further increase the effective length of the SSPP slot. Typically, the minimum fabrication resolution is 0.1 mm in the commercial printed-circuit-board (PCB) manufacturing so that W_{spp2} is fixed as 0.1 mm, and L_{spp2} is limited to 0.38 mm due to the fixed period of SSPP slots. Alternatively, increasing L_{spp1} can efficiently push f_{c-spp} downwards to 30 GHz, as shown in Fig. 2(b), and thus enables narrowband hybrid filter.

At $W_{siw} = 3.76$ mm and $P_{spp} = 0.7$ mm, the original SIW cut-off frequency is at 26.5 GHz. As L_{spp1} increases from 0.33 to 0.53 mm, the SSPP cut-off frequency f_{c-spp} decreases
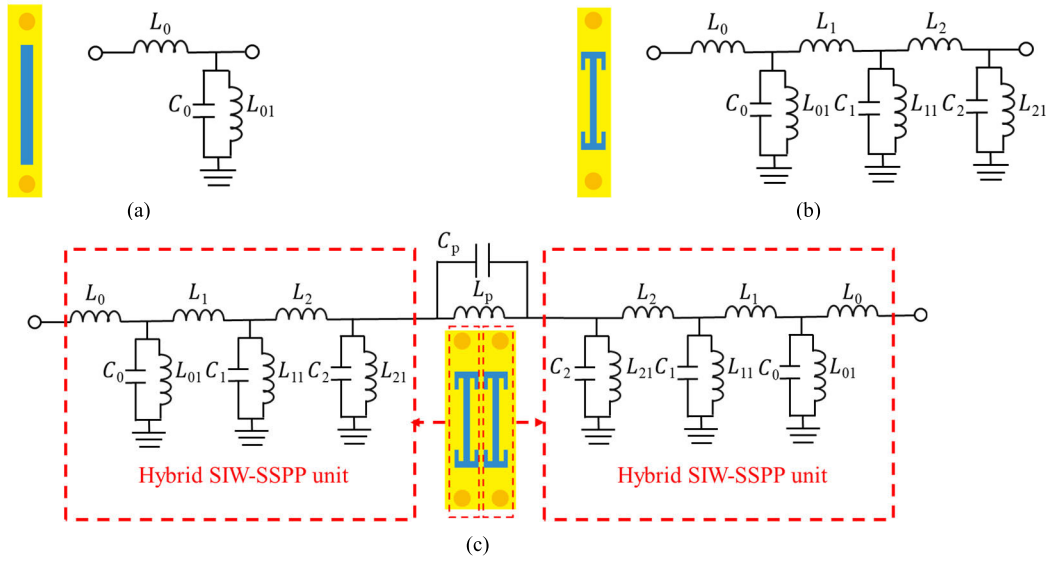
FIGURE 3. The equivalent circuits models of (a) a SIW with a rectangular slot, (b) a SIW with an I-shaped slot, and (c) the proposed hybrid SIW-SSPP filter with I-shaped slots.

from 32.5 to 30 GHz, and the SIW cut-off frequency f_{c-siw} decreases from 26.5 to 25.6 GHz. This phenomenon reveals that the SSPP modes dominate as the cut-off frequencies converge and push the SIW cut-off frequency to low frequencies slightly. The detailed dimensions for an optimized hybrid filter at 30 GHz are listed in Table 1.

B. EQUIVALENT CIRCUIT MODEL

Typically, SIW can be depicted as the classic transmission model with the distributed resistance and inductance in series and capacitance and conductance in parallel, which is the same as the rectangular waveguide [12]. Neglecting the resistive and conductive attenuation, the equivalent circuit of a SIW with a rectangular slot is illustrated in Fig. 3(a). A shunt inductor L_{01} is induced in parallel to the capacitor C_0 by the slot as the current encounters a bend in the slot [28], which corresponds to a bandpass function. In this case, the proposed SIW with the I-shaped slot can be modeled as three L-C parallel resonators cascaded in series, as shown in Fig. 3(b). C_0, C_1, and C_2 are the capacitances induced by the length L_{spp}, L_{spp1}, and L_{spp2} in the I-shaped slot, respectively, and L_{01}, L_{11}, and L_{21} are the corresponding shunt inductances. The values of C_0, C_1, and C_2 can be expressed as [12]:

$$C_0 = \frac{\varepsilon_0 \varepsilon_r \left(W_{siw} - L_{spp} \right) W_{spp1}}{4t}, \tag{5}$$

$$C_1 = \frac{\varepsilon_0 \varepsilon_r \left(W_{siw} - 2L_{spp1} \right) W_{spp2}}{2t}, \tag{6}$$

$$C_2 = \frac{\varepsilon_0 \varepsilon_r \left(W_{siw} - 2W_{spp1} \right) \left(L_{spp2} - W_{spp1} \right)}{4t}, \tag{7}$$

where ε_0 is the vacuum dielectric constant, and t is the substrate thickness. L_0, L_1, and L_2 are the serious inductances for SIW along the signal propagation direction. Figure 3(c) illustrates the equivalent circuit model of the proposed hybrid

SIW-SSPP filter with two I-shape slots. L_p and C_p are the inductance and mutual coupling capacitance between the I-shaped slots.

As L_{spp} gets larger, the capacitance C_0 enlarges, and thus the SSPP cut-off frequency f_{c-spp} red shifts, as shown in Fig. 1(b). Similarly, C_1 enlarges as L_{spp1} increases, leading to a redshift of the SSPP cut-off frequency, as illustrated in Fig. 2(b). Compared to the classic rectangular slot, the I-shaped slot has additional sub-slots to increase the equivalent length, which further reduces the cut-off frequency of the SSPP. Based on the above analysis, the cut-off frequency of the I-shaped SSPPs in the proposed hybrid filter can be expressed as:

$$f_{c-spp} \approx \frac{c_0}{4(L_{spp} + 4L_{spp1} + 2L_{spp2})\sqrt{\varepsilon_{eff}}}. \tag{8}$$

The analytical data of the equivalent circuit in Fig. 3(c) will be discussed together with HFSS simulation in the following section.

C. THREE-DIMENSIONAL SIMULATION

Based on the above eigen mode analysis, 3-D models of SIW, MSL-to-SIW transition, and hybrid filter are built and simulated with absorption boundary in HFSS driven mode, as shown in Fig. 4. The proposed device comprises one SIW and two I-shaped slots on the top electrode of the SIW. The length of SIW L_{siw} is 6.4 mm. To input and output signals, a short taper is designed to connect the hybrid filter and two MSLs, which has been widely used for MSL based interdigital and comb-line filters [29]. The width of the MSLs is chosen as 0.66 mm for 50-Ω impedance, and the length and width of the funnel-shaped taper are denoted as L_t and W_t, respectively.
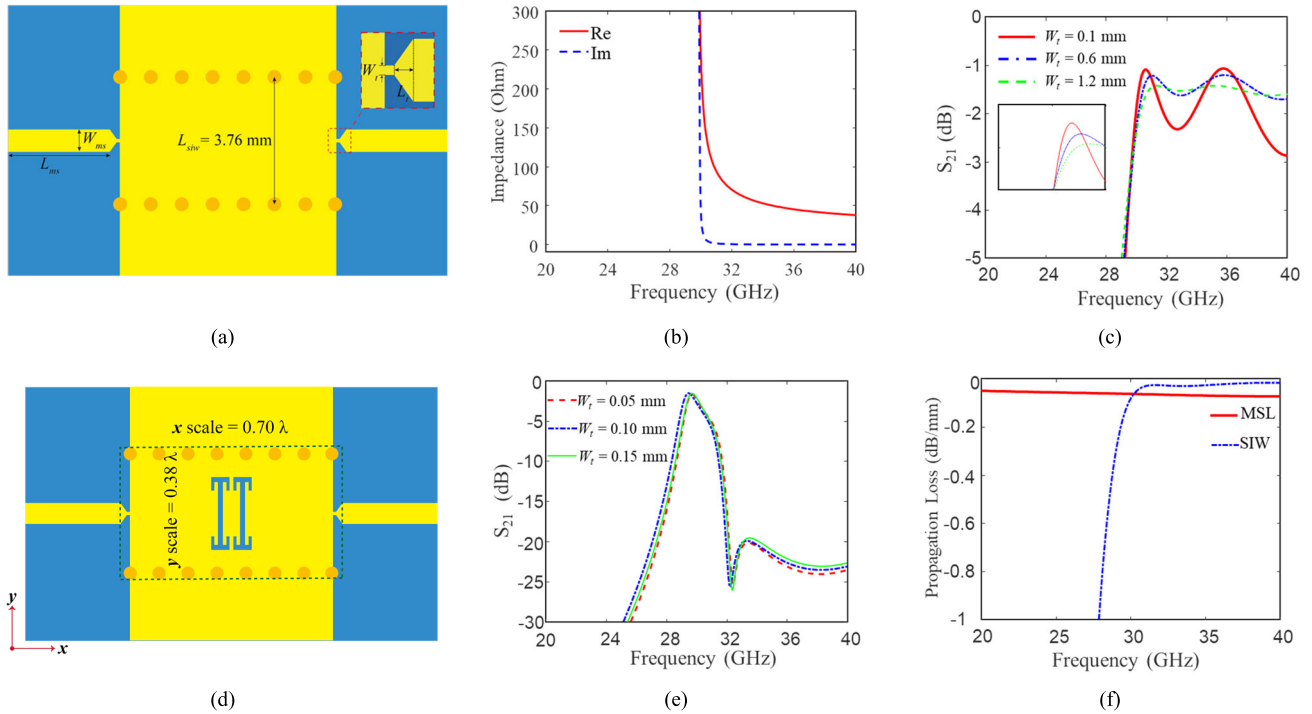
FIGURE 4. Microstrip-to-SIW short taper transition and SIW-SSPP hybrid filter. (a) 3-D driven model of the funnel-shaped sharp transition, (b) simulated effective impedance of SIW, (c) simulated S_{21} with different taper width W_t for the sharp transition, (d) 3-D driven model of the proposed device at 30 GHz, (e) simulated S_{21} with various W_t, and (f) simulated propagation loss of microstrip line and SIW.
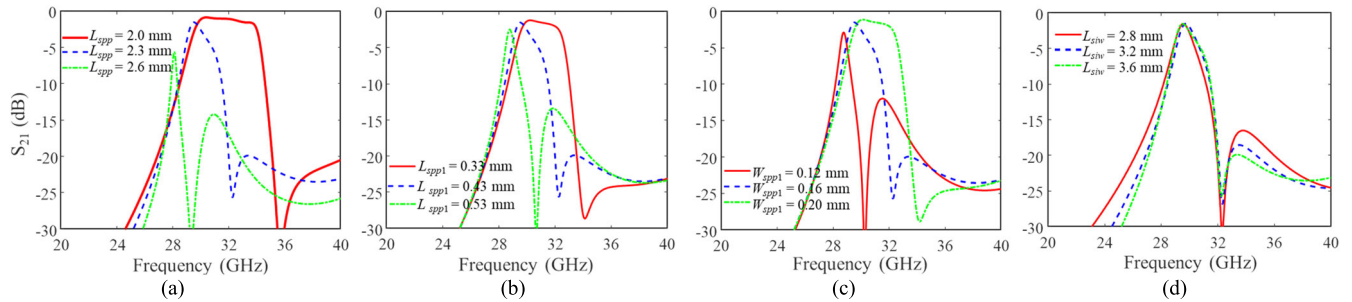

FIGURE 5. Dimension optimization for the proposed SIW-SSPP hybrid filter. (a) L_{spp} variation, (b) L_{spp1} variation, (c) W_{spp1} variation, and (d) L_{siw} variation.

Due to the cut-off response, the effective impedance of SIW ramps fast near the cut-off frequency. To optimize the MSL-to-SIW transition, a short taper structure is investigated, as shown in Fig. 4(a). The width and length of SIW are 3.76 and 6.4 mm, respectively, and the length of MSL is 3 mm. Figure 4(b) illustrates the dispersive effective impedance of SIW, which is as large as 300 Ohms at 30 GHz. In this case, large MSL impedance at small W_t is beneficial for reducing transition loss near the cut-off frequency, as shown in Fig. 4(c). For instance, a flared taper with $W_t = 1.2$ mm is suitable for broadband transition above the cut-off frequency, however, whose insertion loss is relatively large near the cut-off frequency. As W_t decreases, the insertion loss at 30 GHz reduces, which is as small as 1.12 dB at $W_t = 0.1$mm. In this regard, a funnel-shaped sharp taper

with $W_t = 0.1$mm is chosen for the following filter design. In order to analyze the insertion loss of the sharp transition, the attenuation properties of MSL and SIW are simulated, as shown in Fig. 4(f). The propagation loss of the MSL and SIW in Fig. 4(a) and 4(d) is around 0.06 and 0.07 dB/mm at 30 GHz, respectively, and the total propagation loss of MSL and SIW is 0.82 dB. In this case, the insertion loss of a single transition can be estimated as 0.15 dB.

Next, the SIW-SSPP hybrid filter with a funnel-shaped sharp transition in Fig. 4(d) is investigated. Considering the fabrication resolution limit and mechanical stability during fabrication, W_t is further swept for optimizing the proposed device. ± 50-μm fabrication tolerance will not significantly affect the performance of the hybrid filter, as shown in Fig. 4(e). However, the out-of-band reflection increases
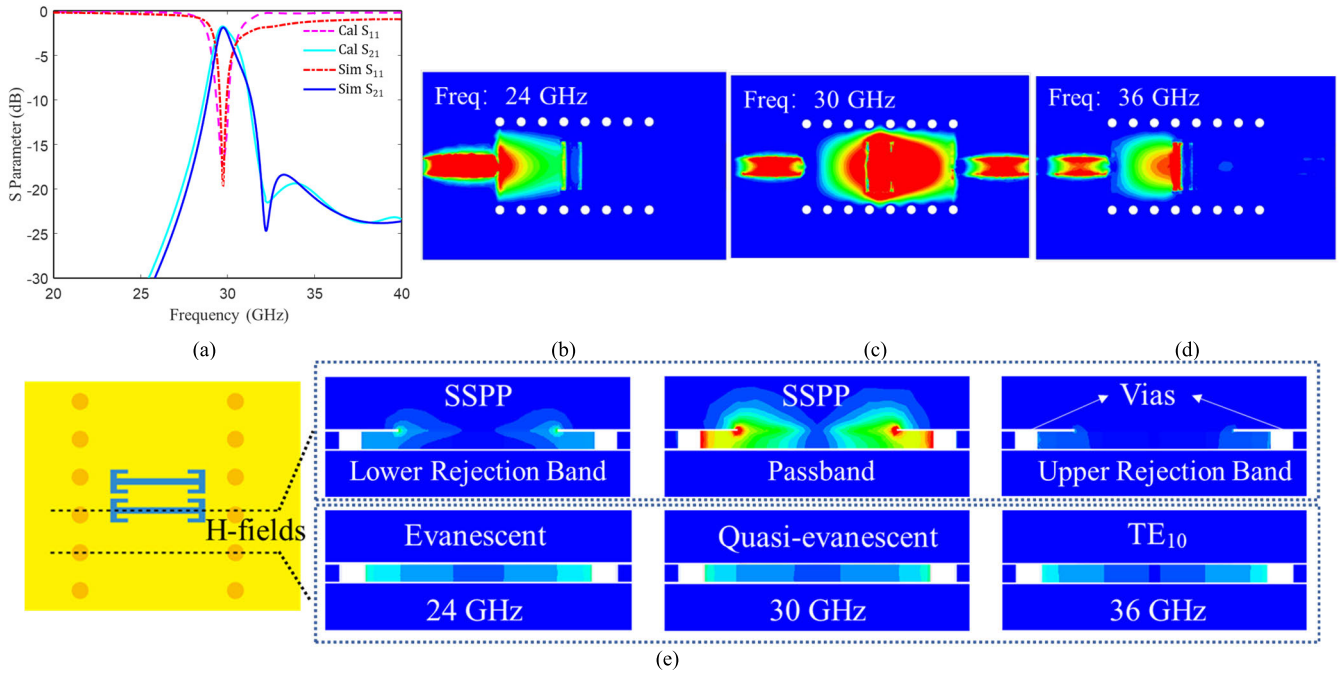
FIGURE 6. Optimized S-parameters and electromagnetic field distributions of the proposed hybrid filter designed at 30 GHz. (a) The simulated S parameters of the proposed narrow passband filter in HFSS and the analytical data of the equivalent circuit model fitted in ADS, simulated electric field distributions at (b) 24 GHz, (c) 30 GHz, and (d) 36 GHz, and (e) simulated magnetic field distributions of the SIW and SIW-SPP hybrid structures.

slightly above 32 GHz as W_t gets larger, which is due to the decreasing impedance of SIW as the frequency increases. In sum, $W_t = 0.1$ mm and $L_t = 0.2$ mm are chosen for the short taper, the latter of which is as small as 0.02λ at 30 GHz. Changing L_t from 0.1 to 0.3 mm does not change the insertion loss at 30 GHz significantly.

In addition, parameter variation of SSPP slots has been studied in Fig. 5. As L_{spp} gets larger, the SSPP cut-off frequency f_{c-spp} red shifts, as shown in Fig. 5(a), which reveals good consistency with the eigen mode simulation in Fig. 1(b). Even if the SSPP cut-off frequency is lower than the SIW cut-off frequency, considerable signals still propagate through the devices due to the SSPP mode, see the green line in Fig. 5(a). Similarly, as L_{spp1} increases, leading to a redshift for the SSPP cut-off frequency, as illustrated in Fig. 5(b). Figure 5(c) depicts the S_{21} variation with respect to the W_{spp1}. As W_{spp1} increases, corresponds to a blue shift of SSPP cut-off frequency. In addition, the S-parameter variation with respect to SIW length is illustrated in Fig. 5(d). As L_{siw} increases, the out-of-band attenuation improves, however, which slightly enlarges the insertion loss.

In sum, L_{spp} is chosen as 2.3 mm, L_{spp1} is chosen as 0.43 mm, and W_{spp1} is chosen as 0.16 mm for the optimized hybrid filter at 30 GHz, as depicted in Table 1. The corresponding S_{11} and S_{21} are shown in Fig. 6(a). It can be noticed that the insertion loss is as low as 1.3 dB at 29.8 GHz, and the 3-dB bandwidth is as narrow as 3% with respect to the center frequency of 30 GHz. The out-of-band attenuation is -20 dB at 27.5 and 31.8 GHz, respectively. The analytical data of the equivalent circuit in Fig. 3(c) are also illustrated in Fig. 6(a),
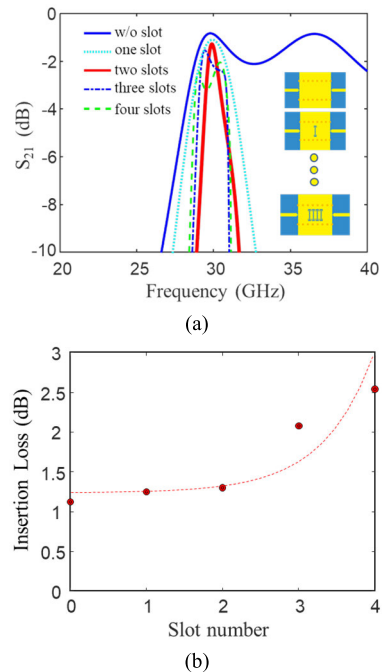
FIGURE 7. Simulated attenuation of the MSL-SIW-MSL structure with various number of SSPP slots. (a) S_{21} with respect to frequency. (b) Attenuation with respect to the SSPP slot number at 30 GHz.

showing good agreement with the full-wave simulation, which is fitted by using Advanced Design System (ADS). Figure 6(b)-(e) illustrates the simulated electric and magnetic field distributions at different frequencies. At 24 GHz, the

TABLE 2. Performance comparison of SIW-SSPP hybrid filters.

Work	Center Freq. /GHz	BW	IL/dB	Length× Width/λ	Lower Band Rejection	Upper Band Rejection	Type
7	20.8	43.8%	>1	3.94×0.46	-20dB@Under 14GHz	-25dB@26.5~30GHz	SIW&2-D SSPP
8	16.7	57.6%	>0.8	3.92×0.49	-25dB@5~12GHz	-20dB@22.3~30GHz	SIW&SSPP in series
9	9.3	44%	>2	2.54×0.48	-20dB@Under 7GHz	-40dB@11.8-19.8GHz	SIW&1-D SSPP
10	5.7	13.3%	>1.7	1.17×0.40	-20dB@5.2~5.4GHz	-20dB@6~6.4GHz	SIW&2-D SSPP
11	12	70%	>1.1	2.68×0.24	-25dB@Under 6.8GHz	-12.5dB@16.5GHz	HMSIW&1-D SSPP
12	23.8	70%	>0.8	4.70×0.32	-25dB@Under 12GHz	-20dB@37~40GHz	HMSIW&1-D SSPP
13	6	59.3%	>1.9	1.90×0.20	-25dB@Under 3GHz	-31.6dB@8.6~16GHz	HMSIW&1-D SSPP
21	3.3	19.2%	>3.6	1.1×0.26	-25dB@Under 3GHz	-34dB@3.7~6GHz	HMSIW&1-D SSPP
22	9.27	60.8%	>0.9	3.01×0.44	-20dB@Under 5.8GHz	-20dB@13.5~20GHz	HMSIW&1-D SSPP
25	8.6	42%	>1.2	1.25×0.63	-25dB@Under 6GHz	-20dB@10.35~15GHz	SIW with U-slot
30	35	13.3%	>1.1	0.16×0.08	-22dB@Under 28GHz	-15dB @42~60GHz	GaAs IPD
31	4.4	8.5%	>1.4	0.5×0.5	-30dB@Under 4GHz	-22dB@4.8~6.8GHz	Microstrip Resonators
32	29.6	4.8%	>1.3	6.39×6.39	-15dB@Under 26GHz	-15dB@32.4-34GHz	Microstrip Resonators
This work	30	3%	>1.5	0.70×0.38	-25dB@Under 26GHz	-17dB@33~60GHz	SIW&1-D SSPP

BW denotes the bandwidth.
IL and RL denote the insertion loss and return loss, respectively.
λ denotes the wavelength at center frequency.

signals are reflected significantly at the interface between the MSL and SIW due to the cut-off response of SIW, as shown in Fig. 6(b). Evanescent waves propagating into the SIW decay exponentially in the Z-direction. At 36 GHz, strong reflection happens right at the I-shaped SSPP slots, which equivalently serves as an open load, showing a good cut-off phenomenon in Fig. 6(d). In contrast, Figure 6(c) shows that the input signals propagate smoothly with little attention at 30 GHz. The magnetic fields of the SIWs and SIW-SSPP hybrid structures at 24, 30, and 36 GHz are illustrated in Fig. 6(e). It can be seen that the SIW mode at 30 GHz is more like the evanescent mode below the cut-off frequency, e.g., at 24 GHz. Furthermore, this evanescent mode shows a similar profile as the hybrid SIW-SSPP mode, which is shown as the 30 GHz field distribution in Fig. 6(e). In this case, little insertion loss is induced between the standard SIW and the SIW with SSPP slots. This is the reason that no transitional SSPP slots are needed in the proposed filter. The evanescent mode of SIW and the surface mode of SSPP attenuate the signal transmission below and above the working frequencies of the proposed filter, respectively.

D. INSERTION LOSS ANALYSIS
As shown in Fig. 4(c) and 6(a), the insertion loss of the MSL-SIW-MSL transition and the proposed hybrid filter is 1.12 and 1.3 dB at 30 GHz, respectively. In this case, the SSPP slots induce little leakage loss for the filter. To investigate the attenuation induced by SSPP slots, hybrid filters with the same dimensions and various numbers of slots are simulated. The S-parameters of the MSL-SIW-MSL structure in Fig. 4(a) with one to four SSPP slots are illustrated in Fig. 7(a). As the slot number increases, the insertion loss gets larger, and the out-of-band rejection gets sharper. The insertion loss at 30 GHz with respect to the slot numbers is illustrated in Fig. 7(b). It can be seen that the insertion loss

increases exponentially, which is mainly due to the evanescent loss of SIW TE_{10} mode near the cut-off frequency. As the slot number increases, the SIW length increases, and thus the loss increases from 1.12 dB to 2.5 dB. To compensate for the bandwidth and insertion loss, the slot number is chosen as two.

III. EXPERIMENTS
A prototype with the optimized dimensions in Table 1 was fabricated, as shown in Fig. 8(a). Due to the fabrication discrepancy, L_{spp} is 2.32 mm, L_{spp1} becomes 0.456 mm, W_{spp1} becomes 0.172 mm, and W_{spp2} becomes 0.125 mm. Here, long MSLs are designed to provide sufficient space for the integration of end-launch connectors. The measurement system setup is illustrated in Fig. 8(b). Two End-launch connectors from Southwest Microwaves Inc. are employed to integrate the fabricated SIW-SSPP hybrid filter with two coaxial lines, and their insertion loss is around 1.5 dB each at 30 GHz as depicted in their datasheet [33]. Vector network analyzer (VNA) Ceyear 3672E is used to characterize the S-parameters of the device under test. Before measurement, VNA is calibrated with calibration kit 85058E by using the standard short-load-open-through (SLOT) method.

The measured S-parameters of the proposed hybrid filter are illustrated in Fig. 8(c), showing good agreement with the simulation data. The measured center frequency is at 29.4 GHz, which has a small red shift compared with the simulated results due to the fabrication tolerance. The minimum insertion loss of the fabricated device is about 4.5dB at 29.4 GHz so that the absolute insertion loss can be estimated as 1.5 dB by removing the loss induced by connectors. This number is 0.2 dB larger than the simulation (1.3 dB), which might be easily introduced by fabrication and integration tolerances. The 3-dB bandwidth of the proposed filter is from 28.8 GHz to 30.2 GHz, which corresponds to 3% with respect to the center frequency.

(a)

(b)

(c)
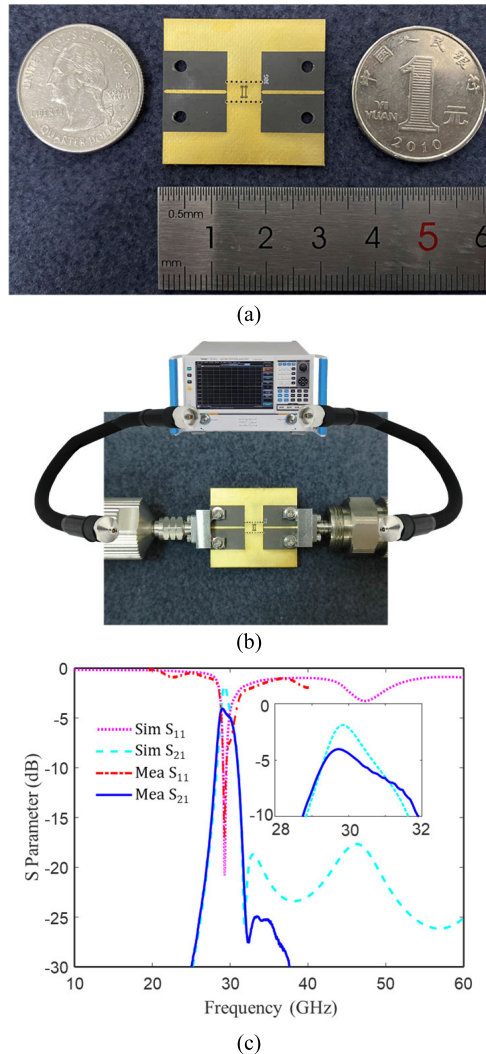
FIGURE 8. Fabricated prototype and its measurement. (a) Top view of the fabricated SIW-SSPP hybrid filter at 30 GHz, (b) measurement system set-up and the device integrated with end-launch connectors, (c) characterized S-parameters.

Table 2 compares the proposed narrowband hybrid filter with the other reported SIW–SSPP hybrid filters [7], [8], [9], [10], [11], [12], [13], [14], [15], [16], [17], [18], [19], [20], [21], [22], [23], [24]. References [11], [12], [13], [21], and [22] have smaller SIW width because they are half mode substrate integrated waveguide (HMSIW). It should be noted that the proposed hybrid filter has the minimum device size and the narrowest bandwidth among the SIW–SSPP hybrid filters. Also, it has little high-order modes due to the high cut-off response of SSPPs and thus shows attractive ultra-wideband out-of-band rejection. The lower out-of-band attenuation is larger than 25dB from 1 to 26 GHz, and the upper out-of-band attenuation is larger than 17 dB from 33 to 60 GHz, as shown in Fig. 8(c). Table 2 also compares our work with the other kinds of narrowband bandpass filters [30], [31], [32]. The proposed filter addresses much narrower passband and much wider rejection band. The out-of-band attenuation can be further improved by adding I-shaped SSPP slots.

IV. CONCLUSION

In this paper, a novel narrowband bandpass filter based on SIW-SPP hybrid structures is proposed. I-shaped SSPP slots are carefully on the top electrode of SIW for converging the cut-off frequencies of SIW and SSPPs. The dispersion properties of the SSPP and SIW units were analyzed in the eigen-mode simulation, and the hybrid structure with MSL feedings and short funnel-shaped transitions was optimized with the driven-mode simulation. No transitional SSPP slots are desired in the hybrid device due to the similar profiles of the quasi-evanescent mode and the SIW-SSPP hybrid mode. A hybrid filter at 30 GHz was fabricated and characterized. The measured insertion loss is 1.5 dB at 29.3 GHz, and the characterized 3-dB bandwidth is as narrow as 3%, i.e., one-order smaller than the other reported SIW-SSPP hybrid filters. The proposed device with narrow passband and broad rejection band is suitable for wideband frequency division multiplexing in advanced communication systems.

REFERENCES

[1] F. Xu, Y. Zhang, W. Hong, K. Wu, and T. J. Cui, "Finite-difference frequency-domain algorithm for modeling guided-wave properties of substrate integrated waveguide," *IEEE Trans. Microw. Theory Techn.*, vol. 51, no. 11, pp. 2221–2227, Nov. 2003.

[2] Y. Zhang, S. Shi, R. D. Martin, and D. W. Prather, "Broadband SIW-to-waveguide transition in multilayer LCP substrates at W-band," *IEEE Microw. Wireless Compon. Lett.*, vol. 27, no. 3, pp. 224–226, Mar. 2017.

[3] A. Belenguer, H. Esteban, and V. E. Boria, "Novel empty substrate integrated waveguide for high-performance microwave integrated circuits," *IEEE Trans. Microw. Theory Techn.*, vol. 62, no. 4, pp. 832–839, Apr. 2014.

[4] D. Deslandes and K. Wu, "Single-substrate integration technique of planar circuits and waveguide filters," *IEEE Trans. Microw. Theory Techn.*, vol. 51, no. 2, pp. 593–596, Feb. 2003.

[5] J. Liu, D. R. Jackson, and Y. Long, "Substrate integrated waveguide (SIW) leaky-wave antenna with transverse slots," *IEEE Trans. Antennas Propag.*, vol. 60, no. 1, pp. 20–29, Jan. 2012.

[6] M. Bozzi, A. Georgiadis, and K. Wu, "Review of substrate-integrated waveguide circuits and antennas," *IET Microw., Antennas Propag.*, vol. 5, no. 8, p. 909, 2011.

[7] D.-F. Guan, P. You, Q. Zhang, K. Xiao, and S.-W. Yong, "Hybrid spoof surface plasmon polariton and substrate integrated waveguide transmission line and its application in filter," *IEEE Trans. Microw. Theory Techn.*, vol. 65, no. 12, pp. 4925–4932, Dec. 2017.

[8] Q. Zhang, H. C. Zhang, H. Wu, and T. J. Cui, "A hybrid circuit for spoof surface plasmons and spatial waveguide modes to reach controllable band-pass filters," *Sci. Rep.*, vol. 5, no. 1, Nov. 2015, Art. no. 16531.

[9] P. Chen, L. Li, K. Yang, and Q. Chen, "Hybrid spoof surface plasmon polariton and substrate integrated waveguide broadband bandpass filter with wide out-of-band rejection," *IEEE Microw. Wireless Compon. Lett.*, vol. 28, no. 11, pp. 984–986, Nov. 2018.

[10] N. Cselyuszka, Z. Sakotic, G. Kitic, V. Crnojevic-Bengin, and N. Jankovic, "Novel dual-band band-pass filters based on surface plasmon polariton-like propagation induced by structural dispersion of substrate integrated waveguide," *Sci. Rep.*, vol. 8, no. 1, p. 8332, May 2018.

[11] D. Guan, P. You, Q. Zhang, Z. Yang, H. Liu, and S. Yong, "Slow-wave half-mode substrate integrated waveguide using spoof surface plasmon polariton structure," *IEEE Trans. Microw. Theory Techn.*, vol. 66, no. 6, pp. 2946–2952, Jun. 2018.

[12] L. Zhao, Y. Li, Z.-M. Chen, X.-H. Liang, J. Wang, X. Shen, and Q. Zhang, "A band-pass filter based on half-mode substrate integrated waveguide and spoof surface plasmon polaritons," *Sci. Rep.*, vol. 9, no. 1, Sep. 2019, Art. no. 13429.

[13] D. Zhang, K. Zhang, Q. Wu, and T. Jiang, "A compact wideband filter based on spoof surface plasmon polaritons with a wide upper rejection band," *IEEE Photon. Technol. Lett.*, vol. 32, no. 24, pp. 1511–1514, Dec. 15, 2020.

[14] M. E. Stewart, "Nanostructured plasmonic sensors," *Chem. Rev.*, vol. 108, no. 2, pp. 494–521, Feb. 2008.

[15] G. Kumar, A. Cui, S. Pandey, and A. Nahata, "Planar terahertz waveguides based on complementary split ring resonators," *Opt. Exp.*, vol. 19, no. 2, pp. 1072–1080, Jan. 2011.

[16] J. B. Pendry, L. Martin-Moreno, and F. J. Garcia-Vidal, "Mimicking surface plasmons with structured surfaces," *Science*, vol. 305, no. 5685, pp. 847–848, Aug. 2004.

[17] Y. Jin Zhou and T. J. Cui, "Broadband slow-wave systems of subwavelength thickness excited by a metal wire," *Appl. Phys. Lett.*, vol. 99, no. 10, Sep. 2011, Art. no. 101906.

[18] M. A. Kats, D. Woolf, R. Blanchard, N. Yu, and F. Capasso, "Spoof plasmon analogue of metal-insulator-metal waveguides," *Opt. Exp.*, vol. 19, no. 16, pp. 14860–14870, Aug. 2011.

[19] H. F. Ma, X. Shen, Q. Cheng, W. X. Jiang, and T. J. Cui, "Broadband and high-efficiency conversion from guided waves to spoof surface plasmon polaritons," *Laser Photon. Rev.*, vol. 8, no. 1, pp. 146–151, Nov. 2013.

[20] Z. Liao, J. Zhao, B. C. Pan, X. P. Shen, and T. J. Cui, "Broadband transition between microstrip line and conformal surface plasmon waveguide," *J. Phys. D, Appl. Phys.*, vol. 47, no. 31, Jul. 2014, Art. no. 315103.

[21] Y. Cui, K.-D. Xu, Y.-J. Guo, and Q. Chen, "Half-mode substrate integrated plasmonic waveguide for filter and diplexer designs," *J. Phys. D, Appl. Phys.*, vol. 55, no. 12, Dec. 2021, Art. no. 125104.

[22] X. Wang, Y. Li, H. Li, and W. Wu, "Broadband filtering Balun employing spoof surface plasmon polariton and substrate integrated waveguide," *AEU Int. J. Electron. Commun.*, vol. 160, Feb. 2023, Art. no. 154511.

[23] H. Ling, Y. Zhang, P. Qian, P. Chen, Y. Shi, Y. Wang, Q. Xin, S. Huan, Q. Wang, and A. Song, "Spoof surface plasmon polariton band-stop filter with single-loop split ring resonators," *Int. J. RF Microw. Comput.-Aided Eng.*, vol. 30, no. 8, May 2020, Art. no. e22267.

[24] M. Salehi and E. Mehrshahi, "A closed-form formula for dispersion characteristics of fundamental SIW mode," *IEEE Microw. Wireless Compon. Lett.*, vol. 21, no. 1, pp. 4–6, Jan. 2011.

[25] R. S. Chen, S.-W. Wong, L. Zhu, and Q.-X. Chu, "Wideband bandpass filter using U-slotted substrate integrated waveguide (SIW) cavities," *IEEE Microw. Wireless Compon. Lett.*, vol. 25, no. 1, pp. 1–3, Jan. 2015.

[26] M. Feng, B. Zhang, H. Ling, Z. Zhang, Y. Wang, Y. Wang, X. Zhang, P. Hua, Q. Wang, A. Song, and Y. Zhang, "Active metal–graphene hybrid terahertz surface plasmon polaritons," *Nanophotonics*, vol. 11, no. 14, pp. 3331–3338, Jun. 2022.

[27] Y. Zhang, S. Shi, R. D. Martin, P. Yao, F. Wang, and D. W. Prather, "Ultra-wideband vialess microstrip Line-to-Stripline transition in multilayer LCP substrate for *E*−and *W*-band applications," *IEEE Microw. Wireless Compon. Lett.*, vol. 27, no. 12, pp. 1101–1103, Dec. 2017.

[28] X. Huo and Z. Li, "Right/left-handed leaky rectangular waveguide with broadside radiation property," *Int. J. Antennas Propag.*, vol. 2021, pp. 1–5, Jan. 2021.

[29] M. M. Najafabadi, S. Vahidi, H. Ghafoorifard, and M. Valizadeh, "Single-channel high-transmission optical band-pass filter based on plasmonic nanocavities," *J. Opt. Soc. Amer.*, vol. 37, no. 8, pp. 2329–2337, Jul. 2020.

[30] H. Yu, Y. Wu, Y. Yang, and W. Wang, "IPD millimeter-wave bandpass filter chip based on stepped-impedance coupled-line dual-mode resonator for 5G application," *IEEE Trans. Circuits Syst. II, Exp. Briefs*, vol. 69, no. 12, pp. 4744–4748, Dec. 2022.

[31] A. Lalbakhsh, A. Ghaderi, W. Mohyuddin, R. B. V. B. Simorangkir, N. Bayat-Makou, M. S. Ahmad, G. H. Lee, and K. W. Kim, "A compact C-band bandpass filter with an adjustable dual-band suitable for satellite communication systems," *Electronics*, vol. 9, no. 7, p. 1088, Jul. 2020.

[32] H.-H. Chou and G.-J. Ke, "Narrow bandpass frequency selective surface with high level of angular stability at Ka-band," *IEEE Microw. Wireless Compon. Lett.*, vol. 31, no. 4, pp. 361–364, Apr. 2021.

[33] B. Rosas, "50 GHz end launch connector test boards," *Microw. J.*, vol. 51, pp. 30–34, Mar. 2008.

BAOQING ZHANG received the B.S. degree in electronic science and technology from the Dalian University of Technology, Dalian, China, in 2018. He is currently pursuing the Ph.D. degree in microelectronics and solid-state electronics with the School of Microelectronics, Shandong University.

His research interests include terahertz spoof surface plasmon polaritons and their active modulation.

ZHAOLIN LI received the B.S. degree in integrated circuit engineering from Shandong University, Jinan, China, in 2020, where he is currently pursuing the master's degree in electronic information.

His current research interest includes microwave and millimeter wave devices.

MENGFA WANG received the B.S. degree in integrated circuit engineering from Shandong University, Jinan, Shandong, China, in 2020, where he is currently pursuing the master's degree in electronic information.

His research interests include microwave and millimeter wave devices, integrated circuits, and the integration of high frequency devices.
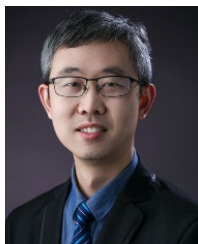
HAOTIAN LING received the B.S. degree in microelectronics science and engineering and the Ph.D. degree in microelectronics and solid-state microelectronics from Shandong University, Jinan, China, in 2015 and 2021, respectively.

He is currently a Research Associate with the QiLu Aerospace Information Research Institute, China. His research interests include terahertz, millimeter wave and microwave functional devices, graphene devices, metal oxide semiconductor devices, metamaterials, and their sensing applications.

YIMING WANG received the B.S. degree in physics and microelectronics, the M.S. degree in physics, and the Ph.D. degree in microelectronics from Shandong University, China, in 2002, 2009, and 2021, respectively.

His research interests include metal oxide semiconductor, thin-film transistors, two-dimensional materials and devices, and high-frequency devices.

XIJIAN ZHANG received the Ph.D. degree in microelectronics and solid-state electronics from Shandong University, Jinan, Shandong, China, in 2006.

He is currently an Associate Professor with the School of Microelectronics, Shandong University. His current research interest includes two-dimensional nanoelectronics devices.

WEIHONG LIU received the B.S. degree in condensed matter physics from Northwest University, Xi'an, China, in 2007, and the Ph.D. degree in microelectronics and solid-state electronics from Xi'an Jiaotong University, Xi'an, in 2011.

Since 2013, he has been an Associate Professor with the Xi'an University of Posts and Telecommunications. From 2018 to 2019, he was a Visiting Scholar with the MMIC Laboratory, Department of Electrical and Computer Engineering, Faculty of Engineering, National University of Singapore. His current research interests include RF integrated circuits design and millimeter-wave devices design.

VICTOR QI received the B.S. degree in electrical engineering from Tianjin University, Tianjin, China, in 1994, the M.S. (M.B.A.) degree from Nankai University, Tianjin, and the Ph.D. degree from the Department of Electrical Engineering, Beijing Institute of Technology, Beijing, China, in 2005.

From 1994 till now, he was with Motorola, Apple, Harman Karden, Mflex, Shure, and AKMMV in the field of wireless communication and high-speed circuit design. He is currently the External Doctoral Supervisor with the South China University of Technology. He was ranked as the leading talent of Suzhou High-Tech Zone, in 2020. He won the honor of outstanding scientific and technical worker in the circuit board industry of Guang Dong province, in 2022. His research interests include the high frequency and high-speed circuit design, mmwave AIP, RF SiP, and the multiphysics simulation of IC packaging.

KUNFENG CHEN is currently a Full Professor with the State Key Laboratory of Crystal Materials, Institute of Novel Semiconductors, Shandong University. His research interests include the growth and application of optoelectronic functional crystal materials for example, $LiNbO_3$ and rare earth single crystals. He has more than 100 publications in peer-reviewed journals.

GONGBIN TANG received the Ph.D. degree in electronics engineering from Chiba University, in 2016, and the Dr.Eng. degree in instrument engineering from Shanghai Jiao Tong University, in 2018. He is currently a Professor with Shandong University, Jinan, China. His research interests include piezoelectric MEMS devices, especially multilayer high performance SAW devices, and their applications to mobile phones. He has contributed to 30 international journal articles and 15 conference proceedings.

AIMIN SONG (Senior Member, IEEE) received the Ph.D. degree from the Chinese Academy of Sciences, in 1995. After three years of fellowships with the University of Glasgow and University of Munich by the Royal Society and Alexander von Humboldt Foundation, he worked with the Nanometre Consortium, Lund University, as a Guest Lecturer, before moving to Manchester as a Lecturer, in 2002. He became a professor in nanoelectronics, in 2006. His research interests include novel nanoelectronic devices and thin-film electronics. His work has led to awards, including ''Researcher of the Year'' Distinguished Achievement Medal of The University of Manchester, Royal Society Brian Mercer Feasibility Award, and a number of best conference paper awards. The potential of practical applications of the nanodevices for printable electronics and energy harvesting have motivated a number of commercialization activities, including 15 patents/patent applications and a spin-out company.

YIFEI ZHANG (Member, IEEE) received the B.S. and M.S. degrees in electrical engineering from the Beijing Institute of Technology, Beijing, China, in 2006 and 2009, respectively, and the Ph.D. degree from the Department of Electrical and Computer Engineering, University of Delaware, DE, USA, in 2016.

He is currently an Associate Professor with the School of Microelectronics, Shandong University, Shandong, China. His research interests include millimeter-wave and terahertz electrical circuits and electronic devices, active metamaterials, microwave-photonic devices, high-frequency integration and packaging, electromagnetic biosensing, and their applications. He has published more than 40 international articles and more than ten patents/patent applications.

○ ○ ○